# Numerical and digital image correlation study of the flexural behavior of prestressed ultra-high-performance concrete beams made from locally available materials

Wei Sun, Brad D. Weldon, Michael J. McGinnis, and Ruinian Jiang

- ■ This paper describes finite element modeling of prestressed ultra-high-performance concrete beams, incorporating a concrete damaged plasticity model, to predict flexural behavior.

- ■ The proposed models use a new approach to apply the prestressing force to the concrete beams within the finite element model with the goal of increasing the accuracy of the models in simulating the prestressing process.

- ■ The numerical models were compared with experimental results from previous studies and determined to accurately predict the flexural behavior of the beams.

Ultra-high-performance concrete (UHPC) is a cementitious material that exhibits compressive strengths equal to or greater than 17 ksi (117 MPa),[1] tensile strengths equal to or greater than 1.16 ksi (8 MPa),[2] exceptional durability, and greater ductility compared with conventional concrete. The material was developed in the mid–20th century; significant research investigating the mechanical behavior of UHPC has been done by various researchers and institutes.[3–5] Various researchers have simulated the mechanical behavior of UHPC using finite element (FE) software. Shafieifar et al.,[6,7] Nasrin and Ibrahim,[8] and Singh et al.[9] performed investigations of the flexural capacity of UHPC beams using Abaqus and demonstrated that the concrete damage plasticity model (CDPM) is effective in predicting the load and moment-carrying capacity of UHPC beams. However, no consistent approach or standard for design and analysis of UHPC is available due to its variable mechanical characteristics, which depend on the mixture proportions—particularly the volume of the fibers. Furthermore, the prestressing process in a concrete beam is difficult to simulate in numerical models using common FE analysis software programs. Therefore, it has been a challenge for researchers to find a suitable numerical model to represent the mechanical behavior of prestressed UHPC.

So far, many efforts have been made to simulate the prestressing process of conventional prestressed concrete

in Abaqus. Wang et al.[10] and Ren et al.[11] used the initial temperature load method to apply the prestress. This approach, which assumes no heat is transferred between the strands and concrete, can be applied to simulate small prestressing loads because the relationship between strain and temperature of the materials is linear when the thermal change of the strands is low. However, a large prestressing force is typically required in many commonly used prestressed concrete members. If the simulated prestressing force is large, requiring a large thermal change (for instance, greater than 212°F [100°C]) to obtain adequate prestressing force, the thermal change will cause the material to experience inelastic behavior, meaning that convergence may not be achieved in the modeling.

Newberry et al.[12] used the initial-stress method to apply prestressing forces on concrete sandwich panels, which applies initial stresses to strands to generate the required prestressing force in the member. Chen et al.[13] also used the initial-stress method to simulate the prestressing force for modeling the structural performance of prestressed UHPC I-girders. This method is effective in providing adequate prestressing force using stress-type initial conditions in Abaqus, but it does not capture how the strands and concrete member deform during the prestressing process. Thus, the initial-stress method is not suitable to express the complete deformation process.

Van Meirvenne et al.[14] modeled the prestressing force as a concentrated force, a body force, and a surface traction to study the force transfer in the end zones of conventional prestressed concrete. The research validated that their model is useful in simulating the friction relationship between strands and concrete, and in deriving related friction coefficients during force transfer. In addition to FE modeling, many current research studies have applied digital image correlation (DIC) techniques to UHPC structures to monitor the deformation process and nondestructive evaluation, which can provide detailed information to verify analytical and numerical models.[15,16]

This paper proposes to analyze prestressed UHPC beams using surface traction in Abaqus to transfer the prestressing force from the strands to the concrete. Also, a modified analytical prediction for the inelastic portions of the tensile and compressive stress and strain behavior of the prestressed UHPC is introduced. Using this approach, this paper will investigate the flexural performance of prestressed UHPC using a CDPM and compare it with experimental results measured by both DIC instrumentation and traditional sensors. The parameters of material characteristics used in the CDPM—for instance, stress-strain behaviors of UHPC and reinforcing steel—are based on the experimental tests done by Giesler et al.[17,18] Note that the materials used in the UHPC were mainly obtained locally in the state of New Mexico. The numerical models are based on scaled, 16 ft (4.9 m) UHPC beams, which were designed to reflect the geometry of one stem of a UHPC channel beam for a bridge.

## The concrete damage plasticity model

The CDPM can generally simulate concrete and other quasibrittle materials that exhibit characteristics of continuum plasticity damage, which is based on the mechanisms of isotropic damaged elasticity in combination with isotropic tensile and compressive plasticity to represent the inelastic behavior of concrete. In Abaqus, yield surface, flow potential, and viscosity parameters are input to simulate the CDPM. The yield criteria used in the CDPM follow the Lubliner et al.[19,20] yield function, which is employed in conjunction with modifications proposed by Lee and Fenves[21] to account for different evolution of strengths under tension and compression. Two constitutive parameters, $K_c$ and $\sigma_{b0}/\sigma_{c0}$, are required to define the yield function $f$. $K_c$ (with a default value of ⅔) is the ratio of the compressive concrete strength under equal biaxial compression to triaxial compression and $\sigma_{b0}/\sigma_{c0}$ (with a default value of 1.16) is the ratio of the initial biaxial compressive yield stress to the initial uniaxial compressive yield stress. The parameter $K_c$ is used to determine the shape of the yield surface in the deviatoric plane based on the full triaxial tests of concrete, while a biaxial laboratory test is necessary to define the value of $\sigma_{b0}/\sigma_{c0}$. The yield function is defined in Eq. (1), and the related parameters $\alpha$, $\psi$, and $\gamma$ are defined in Eq. (2), (3), and (4), respectively.

$$f = \frac{1}{1-\alpha}\left(\overline{q} - 3\times\alpha\times\overline{p} + \psi\times\tilde{\varepsilon}^{pl}\times\overline{\sigma}_{max} - \gamma\left(-\overline{\sigma}_{max}\right)\right) - \overline{\sigma}_c\times\tilde{\varepsilon}^{pl}$$

(1)

where

$\alpha$ = dimensionless constant

$\overline{q}$ = Mises equivalent effective stress

$\overline{p}$ = effective hydrostatic stress

$\psi$ = dilation angle

$\tilde{\varepsilon}^{pl}$ = equivalent plastic strain

$\overline{\sigma}_{max}$ = maximum principle effective stress

$\gamma$ = dimensionless constant

$\overline{\sigma}_c$ = effective compressive cohesion stress

$$\alpha = \frac{\left(\sigma_{b0}/\sigma_{c0}\right)-1}{2\left(\sigma_{b0}/\sigma_{c0}\right)-1} \text{ with } 0 < a < 0.5$$

(2)

$$\psi = \frac{\overline{\sigma}_c^{pl}\left(\overline{\varepsilon}_c^{pl}\right)}{\overline{\sigma}_t\left(\overline{\varepsilon}_t^{pl}\right)}\left(1-\alpha\right)-\left(1+\alpha\right)$$

(3)

where

$\overline{\sigma}_c^{pl}\left(\overline{\varepsilon}_c^{pl}\right)$ = effective compressive cohesion stress

$\overline{\sigma}_t^{pl}\left(\overline{\varepsilon}_t^{pl}\right)$ = effective tensile cohesion stress

$$\gamma = \frac{3\left(1 - K_c\right)}{2K_c - 1} \tag{4}$$

$$\overline{p} = -\frac{1}{3}\overline{\sigma} \times I \tag{5}$$

where

$\overline{\sigma}$      = effective stress tensor

$I$      = first invariant of stress

$$\overline{q} = \sqrt{\frac{3}{2}\left(\overline{S} \times \overline{S}\right)} \text{ with } \overline{S} = \overline{\sigma} + \overline{p} \times I \tag{6}$$

where

$\overline{S}$      = deviatoric part of the effective stress tensor $\overline{\sigma}$

$$G = \sqrt{\left(e \times \sigma_{t0} \times \tan\psi\right)^2 + \overline{q}^2} - \overline{p}\tan\psi \tag{7}$$

where

$G$      = flow potential

$e$      = eccentricity of the plastic potential surface

$\sigma_{t0}$      = initial uniaxial tensile failure stress

$$\sigma_t = \left(1 - d_t\right)E_0\left(\varepsilon_t - \tilde{\varepsilon}_c^{pl}\right) \tag{8}$$

where

$\sigma_t$      = tensile stress

$d_t$      = tensile damage variable

$E_0$      = initial (undamaged) elastic stiffness of material

$\varepsilon_t$      = tensile strain

$\tilde{\varepsilon}_c^{pl}$      = tensile plastic strain

$$\sigma_c = \left(1 - d_c\right)E_0\left(\varepsilon_c - \tilde{\varepsilon}_c^{pl}\right) \tag{9}$$

where

$\sigma_c$      = compressive stress

$d_c$      = compressive damage variable

$\varepsilon_c$      = compressive strain

$\tilde{\varepsilon}_c^{pl}$      = compressive plastic strain

**Figure 1** shows the yield surface in the CDPM. $\sigma_{b0}/\sigma_{c0}$ is used to calculate the parameter $\alpha$ based on Kupfer's curve,[22] which is shown in Fig. 1 right. The $p$-$q$ plane is used to define the flow potential surface and the dilation angle $\psi$ is measured in the $p$-$q$ plane at high confining pressure. $\overline{\sigma}_c\left(\tilde{\varepsilon}_c^{pl}\right)$ and $\overline{\sigma}_t\left(\tilde{\varepsilon}_t^{pl}\right)$ represent the effective tensile cohesion stress and compressive cohe-
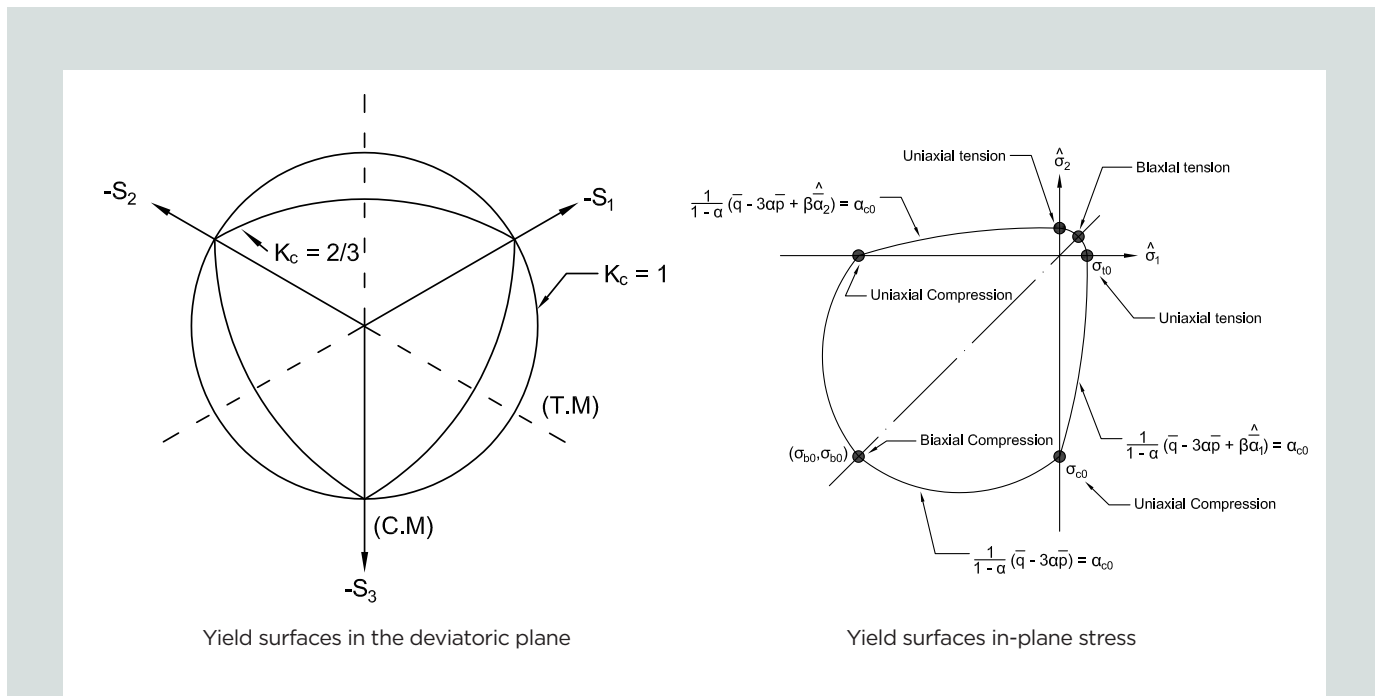


**Figure 1.** Yield surfaces in the deviatoric plane and yield surface in-plane stress. Note: $K_c$ = ratio of compressive concrete strength under equal biaxial compression to triaxial compression; $\overline{p}$ = effective hydrostatic stress; $\overline{q}$ = Mises equivalent effective stress; $\alpha$ = dimensionless constant; $\beta$ = dimensionless constant; $\sigma_{b0}$ = initial biaxial compressive yield stress; $\sigma_{c0}$ = initial uniaxial compressive yield stress.

sion stress, respectively.[21,23,24] $S_1$, $S_2$ and $S_3$ are the yield surfaces on the deviatoric plane. $\hat{\bar{\sigma}}_1$ and $\hat{\bar{\sigma}}_2$ represent the orthogonal uniaxial tensions. $\hat{\bar{\sigma}}_1$ and $\hat{\bar{\sigma}}_2$ are effective uniaxial tensions.

The CDPM assumes nonassociated potential plastic flow. Thus, the flow potential $G$ can be given in the form of Eq. (7), where $\underline{e}$ is the eccentricity of the plastic potential surface with a default value of 0.1. The eccentricity $e$ defines the rate at which the function approaches the asymptote, which indicates that increasing $e$ can provide more curvature to the flow potential. If the confining pressure decreases, the dilation angle will increase. The default value of $e$ ensures that the dilation angle changes only slightly or not at all in a broad range of confining pressure stress. The viscosity parameter $\mu$ is used for the viscoplastic regularization of the concrete constitutive equations in Abaqus/standard analyses. This parameter is ignored in Abaqus/explicit, as rate-dependent analysis is not carried out (default value is 0).

**Figure 2** shows the tensile and compressive behavior of concrete based on the CDPM. The tensile behavior of concrete is linear elastic until the stresses in concrete reach the failure limit $\sigma_{t0}$. The compressive behavior of concrete is nonlinear with gradual softening after its initial yield at $\sigma_{c0}$. In the plastic range, the concrete exhibits compression strain hardening followed by strain softening beyond the ultimate stress $\sigma_{cu}$. The constitutive relationships under uniaxial tension and compression can be expressed by Eq. (8) and (9). The unloading behavior of the concrete specimen exhibits stiffness and strength degradation.[25] The degradation of the elastic stiffness on the strain softening branch of the stress-strain curve is

characterized by two damage variables, $d_t$ and $d_c$ (Eq. [8] and [9]), which are assumed to vary from zero to one. Zero represents that the material is undamaged, while one represents that the material has a total loss of strength.[9] $\varepsilon_c^{el}$ and $\varepsilon_t^{el}$ are elastic tensile and compressive strains.

## Experimental test

Although volumes of research exist on the material properties of UHPC, design standards and specifications for the flexural behavior and moment capacity of UHPC and prestressed UHPC members are not fully developed. To further investigate, improve, and understand the mechanical capability and durability of UHPC, a research program was conducted by Weldon et al.[26] to develop UHPC using local materials. Another study proposed an economical UHPC that achieved enhanced material properties and durability by modifying previously developed nonproprietary UHPC mixture proportions.[27] In addition, Visage et al.[28] and Manglekar et al.[29] presented both an experimental and analytical study on the flexural characteristics of small-scale beams using a locally developed UHPC. A series of large-scale experimental studies were then conducted on UHPC beams and girders, and DIC techniques were employed and performed by Giesler[30] and Manning et al.[31] Based on the previous research performed by Weldon et al.,[26] three prestressed UHPC beams using local materials were fabricated and tested under four-point uniaxial loading by Giesler et al.,[17,18] and these beams were used for the numerical analysis in this paper. The results of the numerical analysis were compared with the experimental results from the previous studies. The mechanical properties
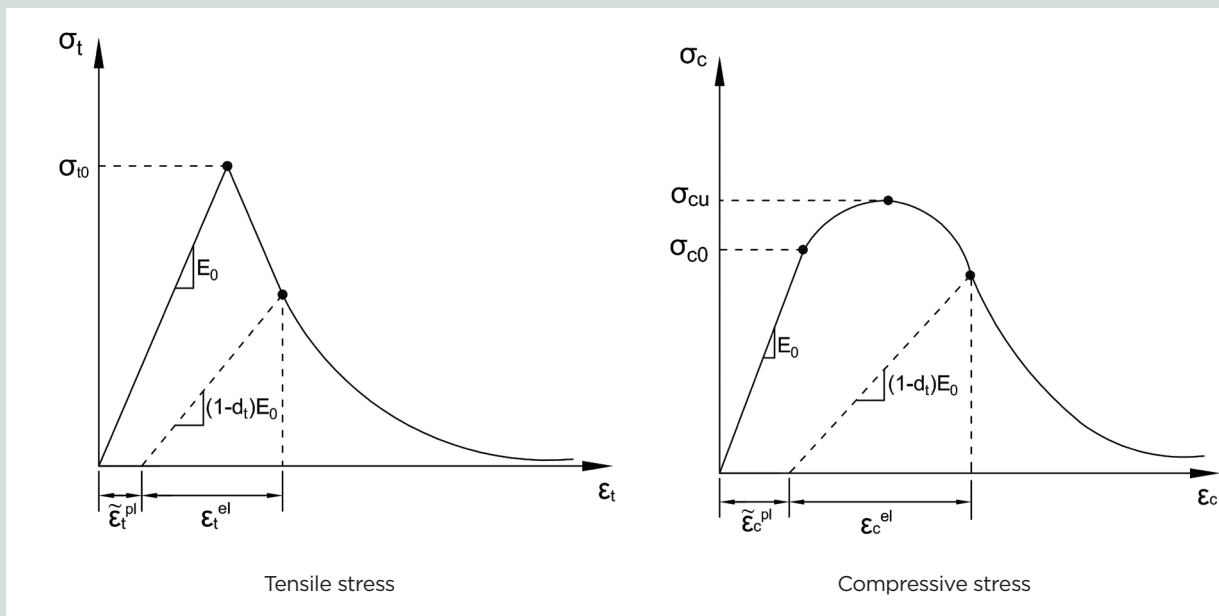


**Figure 2.** Concrete damage plasticity model for concrete under axial tensile and compressive stresses. Note: $d_t$ = tensile damage variable; $E_0$ = initial (undamaged) elastic stiffness of the material; $\varepsilon_c$ = compressive strain; $\varepsilon_c^{el}$ = compressive elastic strain; $\tilde{\varepsilon}_c^{pl}$ = compressive plastic strain; $\varepsilon_t$ = tensile strain; $\varepsilon_t^{el}$ = tensile elastic strain; $\tilde{\varepsilon}_t^{pl}$ = plastic strain; $\sigma_c$ = compressive stress; $\sigma_{c0}$ = initial uniaxial compressive yield stress; $\sigma_{cu}$ = the ultimate compressive stress; $\sigma_t$ = tensile stress; $\sigma_{t0}$ = initial uniaxial tensile failure stress.

of the materials, such as the reinforcing steel and UHPC, used in this analysis are based on Giesler et al.[17,18]

## Materials

In this study, most of the constituents of the mixture proportions used for the nonproprietary UHPC were locally available materials, except the steel fibers and high-range water-reducing admixture (HRWRA), which were obtained from a national distributor. To obtain the required design compressive strength of 22.0 ksi (152 MPa) for the UHPC, a water–cementitious material ratio (w/cm) of 0.145 and 1.5% steel fiber by volume were used. The monofilament, straight fibers were 0.008 in. (0.20 mm) in diameter and 0.50 in. (13 mm) in length, which resulted in a length-to-diameter aspect ratio of 65. The fibers had a 285 ksi (1965 MPa) minimum tensile strength with a modulus of elasticity of 29,000 ksi (200 GPa). The mixture proportions can be found in Giesler.[30] The modulus of elasticity $E_c$ of the UHPC was 6065 ksi (41.82 GPa), which was proposed by Guaderrama and Weldon[32] based on experimental tests.

No. 3 (10M) mild steel bars were used for the compression reinforcement and stirrups in beam specimens. Tension tests were performed on four samples of the reinforcing bars. An average yield stress of 63.7 ksi (439 MPa), an average maximum stress of 97.6 ksi (673 MPa), and an average modulus of elasticity of 26,600 ksi (183 GPa) were obtained.

The prestressing strands used in the beam specimens were 0.6 in. (15.2 mm) diameter Grade 270 (1860 MPa) low-relax-ation strands. The yield strength of the strands $f_{py}$ was taken as 245.0 ksi (1689 MPa), which is 90% of the ultimate strand tensile strength fpu ($f_{py} = 0.90 f_{pu}$) in accordance with the *AASHTO LRFD Bridge Design Specifications*.[33] The modulus of elasticity of the strand was provided in the supplier's specifications as 28,800 ksi (199 GPa).

For the composite (T section) beam described in the following section, the deck was a cast-in-place composite high-strength concrete (HSC) deck. The HSC compressive strain at crushing was assumed to be 0.003, which followed the AASHTO recommendations.[33] The ultimate compressive strength of the HSC was measured to be 8.0 ksi (55 MPa). Welded-wire reinforcement with grid dimensions of 4.0 × 4.0 in. (100 × 100 mm) was placed at midheight in the deck. The diameter of the wires was 0.22 in. (5.6 mm). Based on the experimental tests, an average yield stress of 65 ksi (448 MPa), a tensile strength of 75 ksi (517 MPa), and a modulus of elasticity of 29,000 ksi (200 GPa) were measured for the wire mesh.

## Description of the beam specimens

In the experimental program, three 16 ft (4.9 m) nonproprietary UHPC beams with similar cross sections were designed to investigate their flexural performance. The reinforcement in the beams varied and one beam specimen included a composite deck. Beam 1 was a prestressed UHPC rectangular cross section without shear stirrups (**Fig. 3**). Beam 2 was a prestressed UHPC rectangular cross section with shear stirrups meeting AASHTO requirements (Fig. 3). Beam 3 was a prestressed UHPC rectangular cross section with a composite
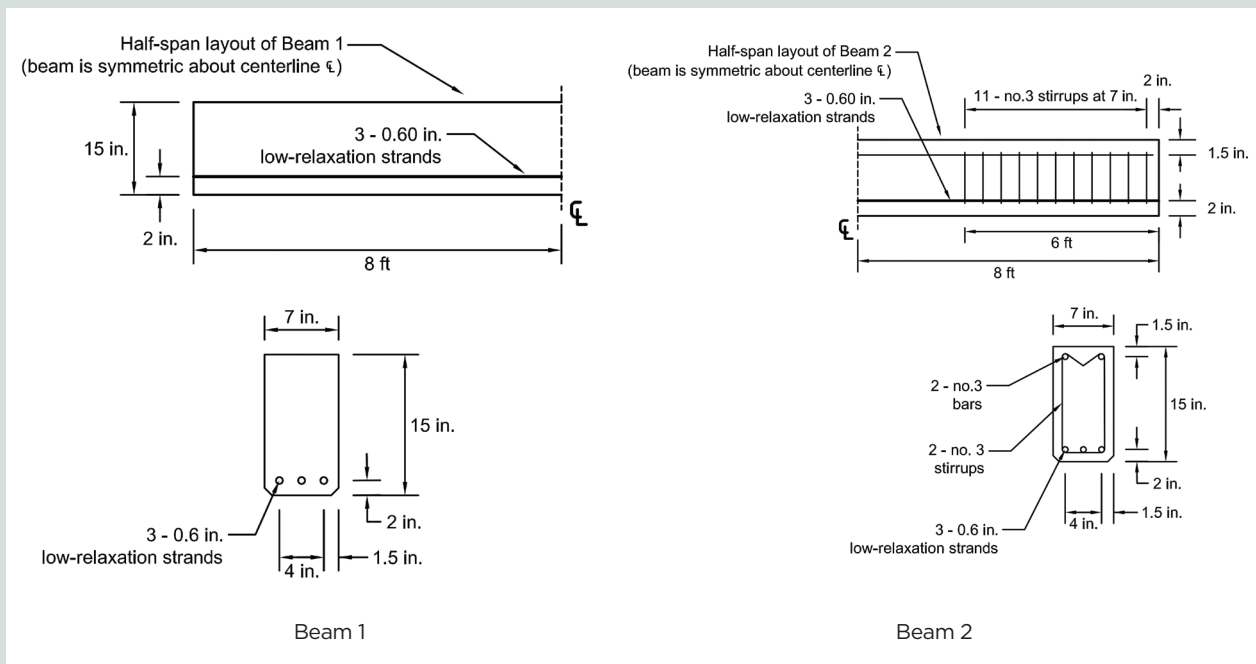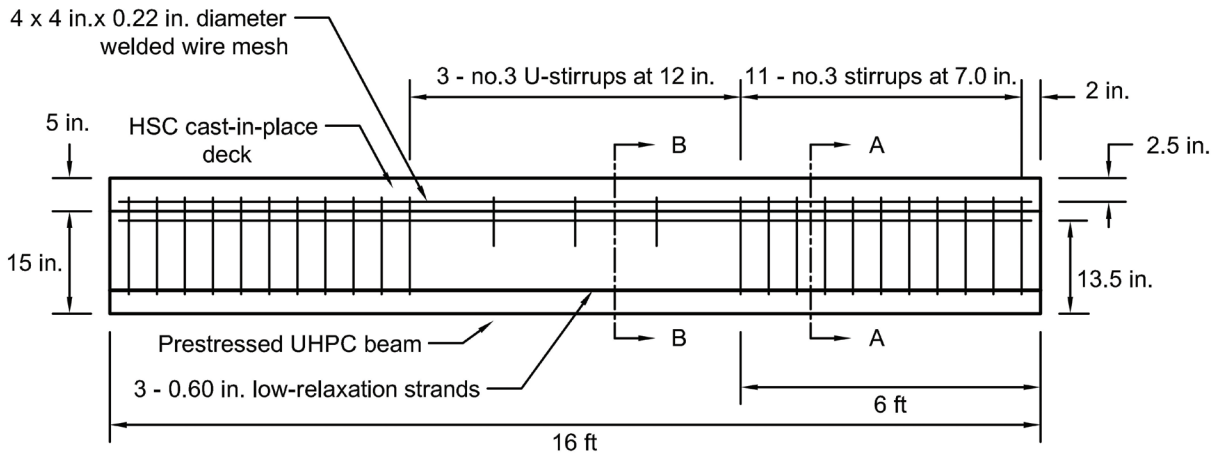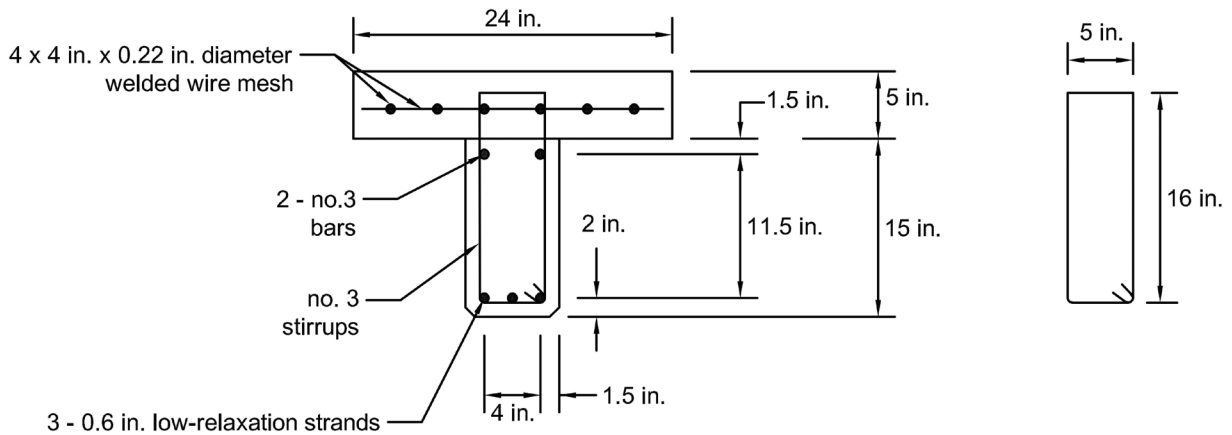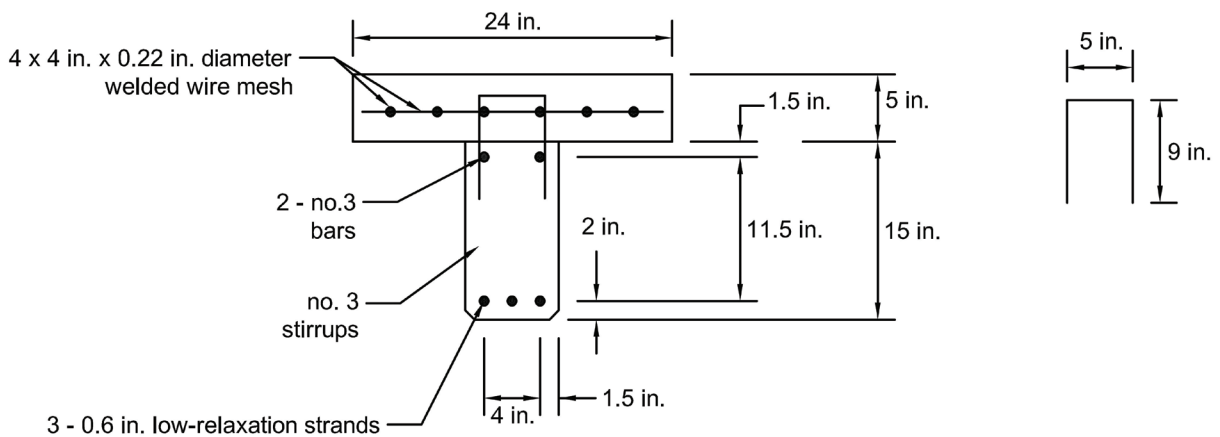


**Figure 3.** Half-span profile view and cross-section of beam 1 and beam 2. Source: Giesler et al., 2014. Note: Not to scale. 1 in. = 25.4 mm; 1 ft = 0.305 m; no. 3 = 10M.

**Figure 4.** Beam 3 profile view and cross-section views. Source: Giesler, 2014. Note: Not to scale. HSC = high-strength concrete; UHPC = ultra-high-performance concrete. 1 in. = 25.4 mm; 1 ft = 0.305 m; no. 3 = 10M.

HSC deck, and shear stirrups, U stirrups, and a wire mesh[30] all designed according to AASHTO requirements (**Fig. 4**). The rectangular cross sections of the beams had a width of 7.0 in. (178 mm) and a height of 15.0 in. (381 mm). Beams 1, 2, and 3 had one layer of prestressing strands, consisting of three 0.6 in. (15.2 mm) diameter low-relaxation strands placed 2.0 in. (50 mm) from the bottom face of the beam. The reinforcement details of beam 3 were similar to beam 2; however, a composite cast-in-place HSC deck was placed and attached to the beam through the composite action of the reinforcement. The depth of the deck was 5.0 in. (127 mm), and welded-wire reinforcement with grid dimensions of 4.0 × 4.0 in. (100 × 100 mm) was placed in the deck. In addition, three U-shaped stirrups were placed near the midspan to prevent any separation of the deck within the pure moment region.

Due to the lack of design guidance or specifications, and to ensure that failure at prestress transfer would not occur, the beam sections shown in Fig. 3 and 4 were designed assuming no fiber contribution to the tensile resistance. For the beams with stirrups, the design procedure followed the AASHTO LRFD specifications[33] and resulted in 11 no. 3 (10M) stirrups at 7.0 in. (178 mm) spacing, beginning 2.0 in. (50 mm) from each end face of the specimen. Near the midspan of the beam, no shear reinforcement was included to limit its effect on the flexural behavior.[17,18]

## Test setup and loading

Four-point loading tests were conducted on the beam specimens. The test setups, instrumentation, and loading points were kept constant for the three beams. **Figure 5** shows the
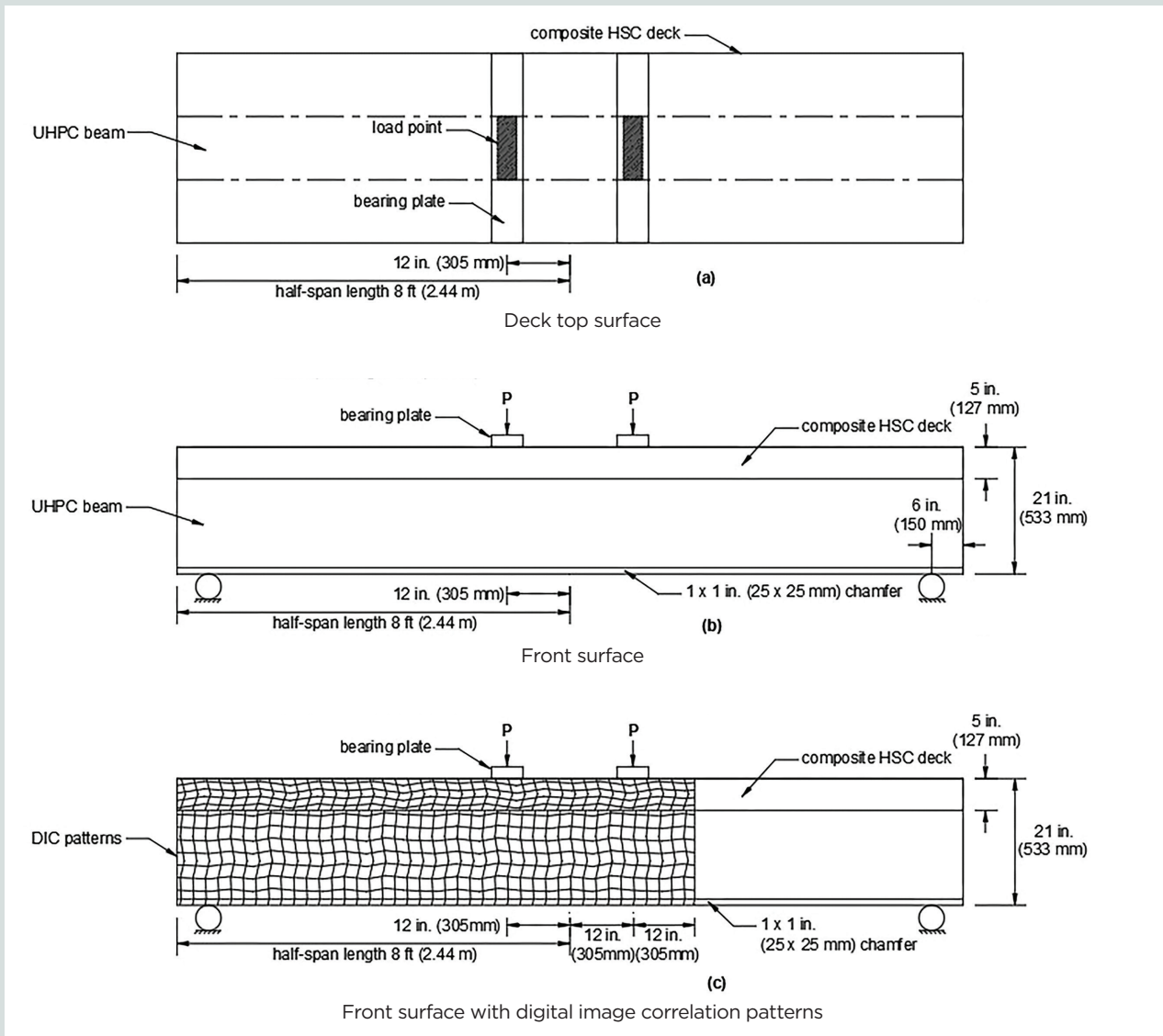


**Figure 5.** Test setup and loading points for Beam 3. Source: Giesler, 2014. Note: Not to scale. DIC = digital image correlation; HSC = high-strength concrete; *P* = applied vertical load in four-point loading test; UHPC = ultra-high-performance concrete. 1 in. = 25.4 mm; 1 ft = 0.305 m.

test setup for beam 3. The effective prestressing force of beams 1, 2, and 3 measured by embedded vibrating wire strain gauges was, respectively, 86.9, 94.0, and 83.0 kip (387, 418, and 369 kN) before load was applied to the specimen.[30]

To investigate the local behavior of the beam, two DIC systems were applied to capture changes in strain, one with a pixel density of 1624 × 1236 and one with a pixel density of 1280 × 1024. The regions of the DIC patterns for collecting data applied on all beams were similar (Fig. 5).

## Numerical model

### Material parameters used in the numerical model

Because the numerical model is simulated to predict the behavior and guide the design of prestressed UHPC structures, the tensile and compressive behavior of the UHPC, the prestressing strands, and mild steel reinforcement (reinforcing bars and stirrups) obtained from material tests are essential components for defining the material model. **Table 1** shows the material properties used in the numerical model of the prestressed UHPC beams, which were based on the previous experimental tests conducted by Giesler et al.[17,18] **Figure 6** shows the adopted tensile and compressive stress-strain responses of the UHPC. In Fig. 6, the inelastic portions of the material behaviors are assumed to be linearly decreasing because only yield strain, ultimate strain, and crushing strain were available from the material property tests. Therefore, piecewise linear variations on the two curves were assumed for the inelastic responses of the UHPC, and an analytical stress-strain behavior for UHPC in both compression and tension is assumed (Fig. 6).

### Finite element modeling

In this research, the CDPM was used in the FE model for simulations with Abaqus. Table 1 shows the material parameters (UHPC, prestressing strands, and mild steel reinforcement) used for the CDPM. To study the flexural behavior of the prestressed UHPC beams, three three-dimensional (3-D)

models were built to simulate the behavior of the experimentally tested beams (**Fig. 7**).

An eight-node reduced integration linear brick (C3D8R) was used to mesh the UHPC beams and prestressing strands. For beams 1 and 2 (Fig. 7) the mesh size of the UHPC was 8 × 1.75 × 1.56 in. (203 × 44.5 × 39.6 mm) (the beam dimensions were 192 × 7 × 15 in. [4880 × 178 × 381 mm]). Eight seeds were used to mesh the circular cross section of the strands (0.6 in. [15.2 mm] diameter), and the mesh size for the strands in length was 8 in. In addition, four steel plates were used as bearing plates for applying the loads, as well as at the supports. The plates (3 × 7 × 1 in. [76 × 178 × 25 mm]) were meshed with the eight-node reduced integration linear brick (C3D8R). The mesh size of the plates was 0.5 × 1 × 0.3 in. (13 × 25 × 8 mm). For beam 3 (Fig. 7), the mesh size of the UHPC for the web was 1.92 × 1.17 × 1.56 in. (48.8 × 29.7 × 39.6 mm) (the beam web dimensions were 192 × 7 × 15 in. [4880 × 178 × 381 mm)]. The mesh size for the flange of the beam was 1.92 × 2.13 × 1.25 in. (48.8 × 54.1 × 31.8 mm) (the beam flange dimensions were 192 × 24 × 5 in. [4880 × 610 × 127 mm]). The mild steel reinforcement (reinforcing bars and stirrups) were created through the 3-D wire elements, which were assumed to be perfectly bonded with the UHPC (3-D solid elements). Thus, the embedded constraint was used as the interaction between the mild steel reinforcement and the UHPC. In addition, four steel plates were added as bearing plates for applying the loads, as well as for the supports.

### Stages of applying prestressing force and vertical loads

This research used a new approach to apply prestressing force to simulate the prestressing process, which not only transfers prestress to the concrete beam but also allows the deformation of the beam due to the prestressing force (that is, camber) to be simulated. The prestressing force was applied using surface traction in Abaqus. The total prestressing force $P_{st}$ was applied satisfying Eq. (10):

$$P_{st} = \overrightarrow{\sigma}_{st} \times A_{surface} \tag{10}$$

| Table 1. Material parameters of prestressed ultra-high-performance concrete used for the numerical model based on experimental results | | | | |
|---|---|---|---|---|
| **Elastic properties** | | | | |
| **Modulus of elasticity** | | **Poisson's ratio** | | |
| 6065 ksi | | 0.18 | | |
| **Plastic properties** | | | | |
| **Dilation angle $\psi$** | **Eccentricity $e$** | **$\sigma_{bo}/\sigma_{co}$** | **$K_c$** | **Viscosity** |
| 50 | 0.1 | 1.1 | 0.66 | 0 |

Note: $K_c$ = ratio of compressive concrete strength under equal biaxial compression to triaxial compression; $\sigma_{bo}$ = initial biaxial compressive yield stress; $\sigma_{co}$ = initial uniaxial compressive yield stress. 1 ksi = 6.895 MPa.
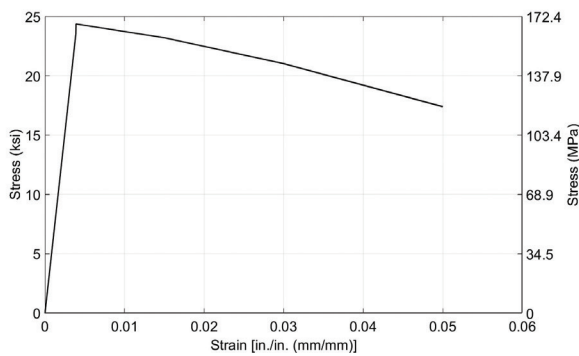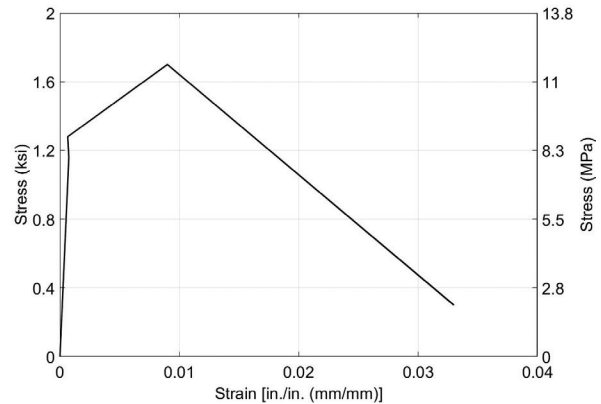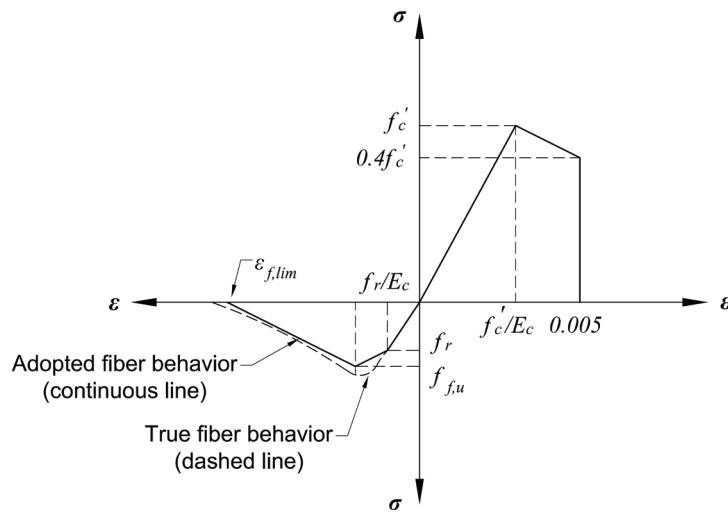
**Figure 6.** Adopted compressive and tensile behavior of ultra-high-performance concrete (UHPC) based on experimental tests and assumed analytical stress-strain behavior for UHPC in both compression and tension. Note: Not to scale. $E_c$ = modulus of elasticity of concrete; $f'_c$ = concrete compressive strength; $f_{f,u}$ = tensile strength of the crack bridging fibers; $f_r$ = concrete modulus of rupture; $\varepsilon$ = strain; $\varepsilon_{f,lim}$ = limiting strain for fiber postcracking strength; $\sigma$ = stress.

where

$P_{st}$ = prestressing force on the prestressing strands

$\overrightarrow{\sigma_{st}}$ = applied surface traction on the prestressing strands

$A_{surface}$ = curved surface area of the prestressing strands

Because $\overrightarrow{\sigma_{st}}$ is a vector, the surface traction stresses are applied on each half-length of the strands in opposite directions (**Fig. 8**). Thus, based on Eq. (10), the applied stresses on the strands due to the prestressing force for beams 1, 2, and 3 were 160 , 173, and 153 psi (1.10, 1.19, and 1.05 MPa), respectively. In addition, the interactions between the prestressing strands and the UHPC were defined as tie connections to ensure that the prestress could be effectively transferred to the UHPC. The

surface traction was applied on the strands in increments so that the transfer of prestressing force was captured (**Fig. 9**).

## Numerical results of the simulation

Figure 9 shows the prestressing simulation, capturing the camber and flexural deformation. **Figure 10** shows the load-deflection responses at midspan from the experimental tests and numerical models. A 0.16 in. (4.0 mm) negative deflection (Fig. 9) occurred in the rectangular beam without stirrups due to prestress. A 0.09 in. (2.3 mm) negative deflection (Fig. 9) occurred in the rectangular beam with stirrups, and a 0.07 in. (1.8 mm) negative deflection (Fig. 9) occurred in the T beam. To present the actual relationship between applied load and deflection, the camber deflection offset was added to the flexural portion of the numerical deflection data.
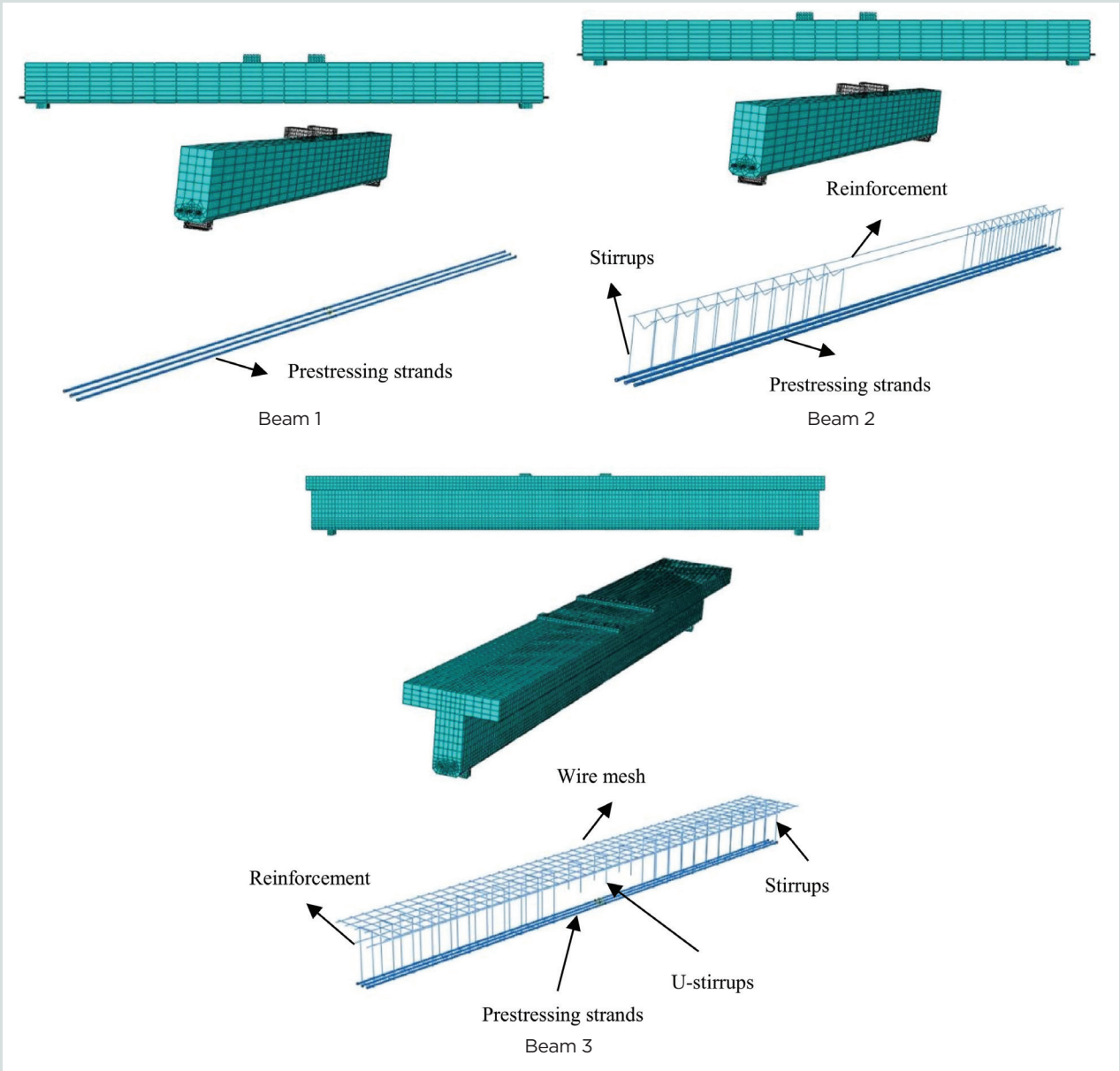
**Figure 7.** Three-dimensional models of prestressed ultra-high-performance concrete beams and reinforcement layout.
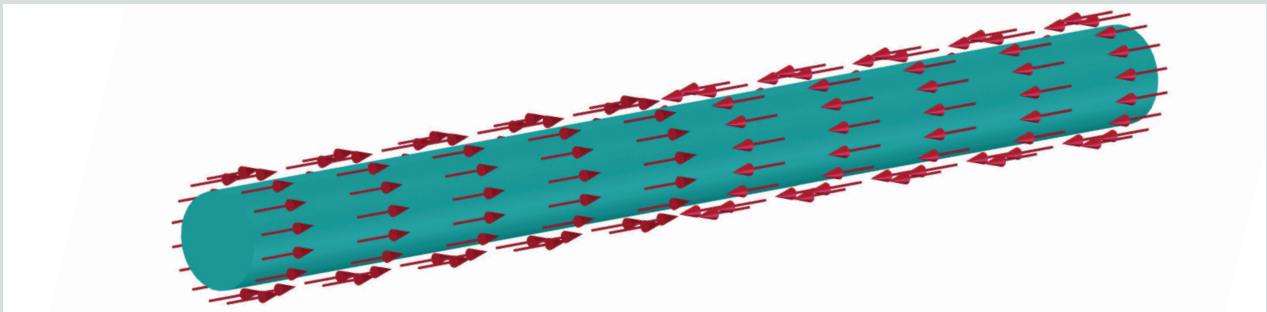


**Figure 8.** Directions of surface traction applied per strand
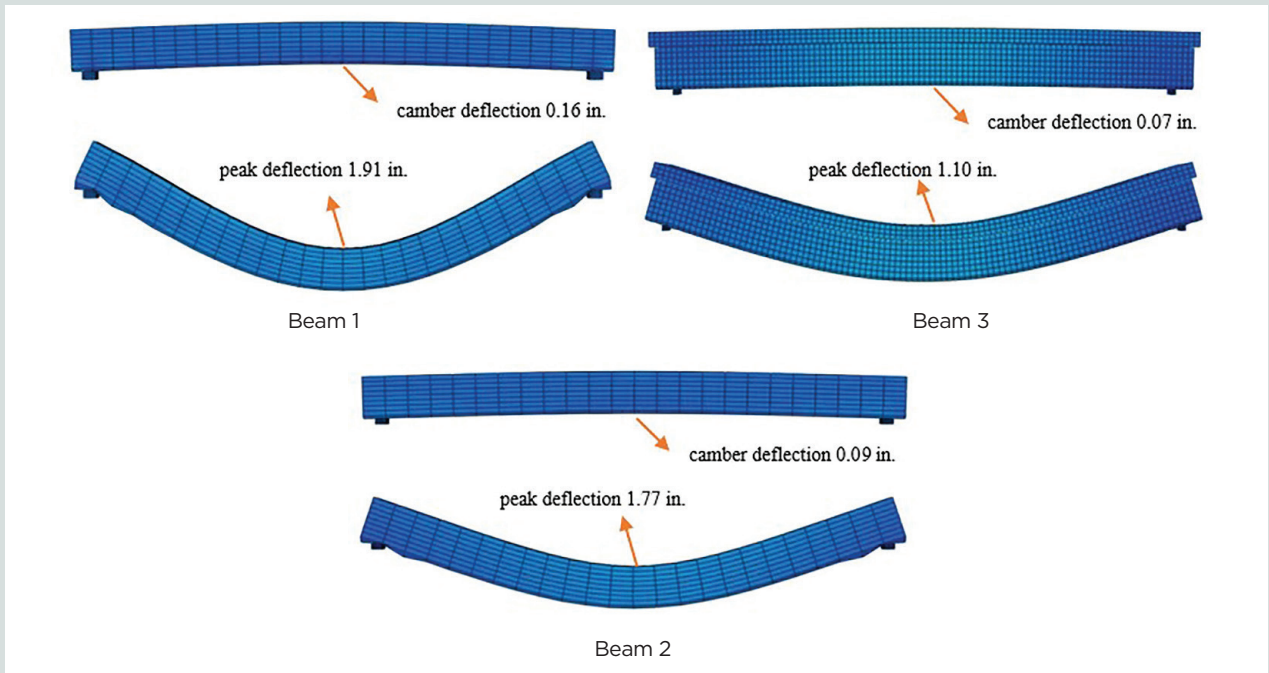
**Figure 9.** Prestressing process and flexural deformation of beams. Note: Not to scale. 1 in. = 25.4 mm.
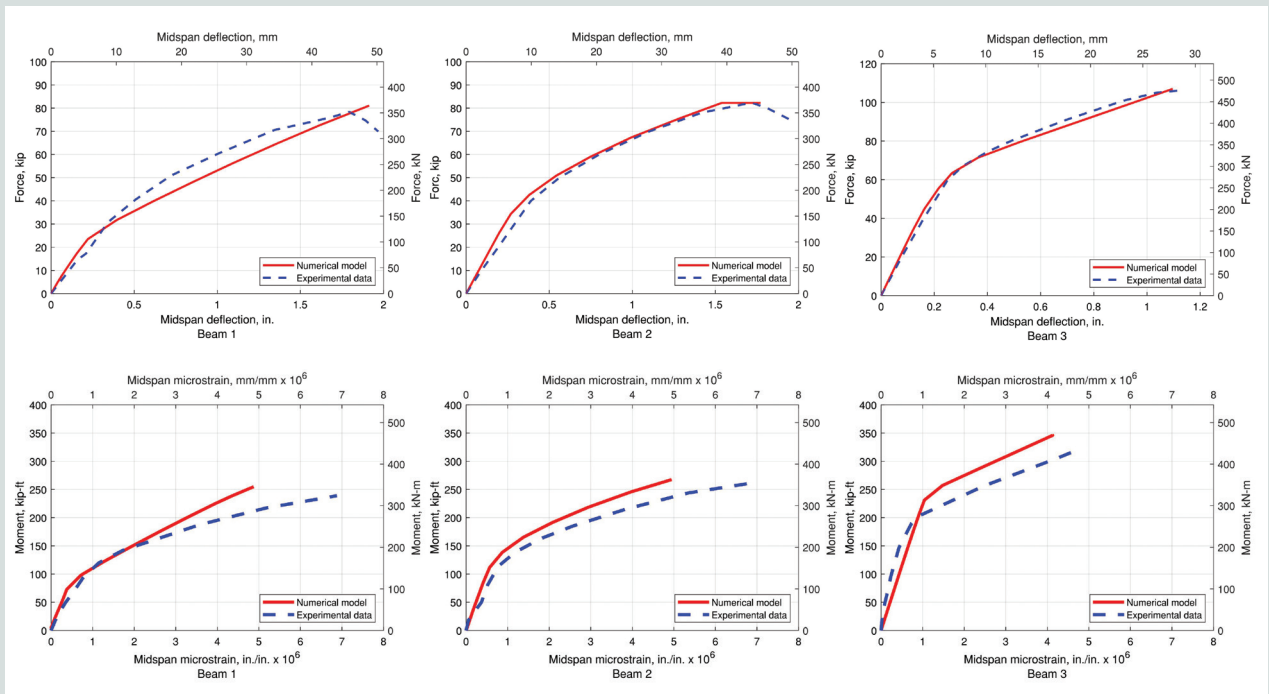


**Figure 10.** Beam deflection response at midspan compared with load and midspan moment compared with microstrain at 13.5 in. from the top surface. Note: 1 in. = 25.4 mm.

The models show good accuracy in predicting the deformation due to prestress, peak vertical load, and corresponding deflection at midspan of the beam when compared with the experimental tests. **Table 2** shows the camber deflection, peak load, and peak deflection from experimental tests and numerical simulation. **Table 3** shows the captured DIC visualization of the behavior of UHPC beams under peak load and their numerical simulation. Figure 10 shows the moment-microstrain
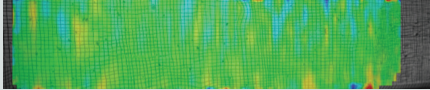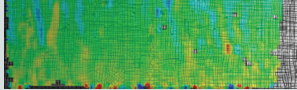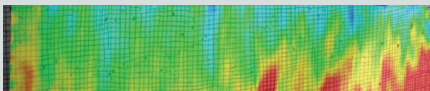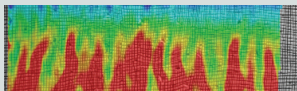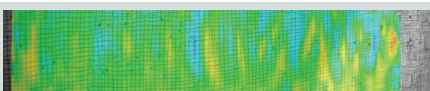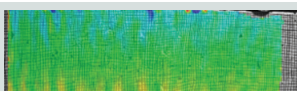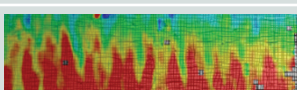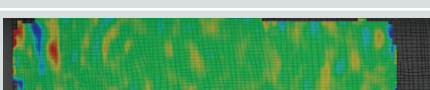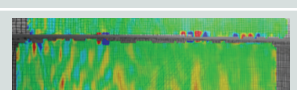
**Table 2.** Camber deflection, peak load, and peak deflection from experimental test and numerical model

| Model | Camber deflection, in. | | Peak load, kip | | Peak deflection, in. | |
|---|---|---|---|---|---|---|
| | Experimental test | Numerical model | Experimental test | Numerical model | Experimental test | Numerical model |
| Beam 1 | 0.19 | 0.16 | 78.4 | 81 | 1.80 | 1.91 |
| Beam 2 | 0.19 | 0.09 | 82.3 | 84.5 | 1.73 | 1.77 |
| Beam 3 | 0.13 | 0.07 | 107 | 108.5 | 1.16 | 1.10 |

Note: 1 in. = 25.4 mm; 1 kip = 4.448 kN.

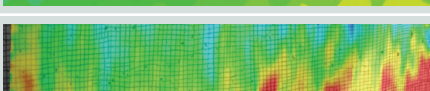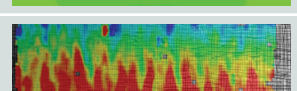**Table 3.** Digital image correlation visualization and numerical simulation of ultra-high-performance-concrete beams at first cracking and under peak load

| Beam section | Time | Specimen/model | Load, kip | Shear region | Pure moment region |
|---|---|---|---|---|---|
| 1 | First cracking | Experimental specimen, | 35.5 |  |  |
| | | Numerical model | 23.8 |  |  |
| | Peak load | Experimental specimen | 78.4 |  |  |
| | | Numerical model | 81 |  |  |
| 2 | First cracking | Experimental specimen | 39.5 |  |  |
| | | Numerical model | 35.4 |  |  |
| | Peak load | Experimental specimen | 82.3 |  |  |
| | | Numerical model | 84.5 |  |  |
| 3 | First cracking | Experimental specimen | 56.2 |  |  |
| | | Numerical model | 46.8 |  |  |
| | Peak load | Experimental specimen | 107 |  |  |
| | | Numerical model | 108.5 |  |  |

Note: 1 kip = 4.448 kN.

curves at 13.5 in. (343 mm) from the top surface of the beams at midspan, and **Figure 11** shows the depth of the neutral axis compared with deflection at midspan. The trends of numerical simulation and DIC data are similar. In Table 3, the color spectrum in the images represents changes in the strain in the beams' longitudinal surface. The location of the neutral axis from numerical simulation was lower than shown in the DIC data because the DIC strains captured the cracking in the concrete in the experimental tests. The CDPM in Abaqus can only characterize the deterioration of modulus of elasticity using the damage parameter and plastic strain; the crack width cannot be simulated. This resulted in the numerically simulated peak strains being slightly less than the DIC data, and the location of the neutral axis was also lower than shown in the DIC data.

## Conclusion

The objective of this research was to numerically model the flexural behavior of prestressed UHPC beams through FE analysis and compare the model with the experimental data to verify the effectiveness of the numerical model in predicting the flexural performance of the prestressed UHPC beams. The material parameters used in the numerical model and the data for the flexural experimental behavior were adopted from the tests conducted by Giesler et al.[17,18] The inelastic tensile and compressive stress-strain relationship used in the models were piecewise linear.

The comparison of numerical and experimental results shows that load capacity, initial stiffness, deflection at peak load,

and strain at peak load of the numerical model are in good agreement with the experimental results. This implies the following:

- The numerical models are validated to simulate the flexural behavior of prestressed UHPC beams. The results show that the force-deflection curves of the numerical models are within 5% of the experimental data. The slight differences observed between the experimental results and the analytical model, particularly for beam 1, which relied solely on the steel fibers for shear resistance, can be attributed to the random nature of the steel fibers. The behavior of steel fibers in UHPC beams cannot be accurately simulated through static analysis in Abaqus. Therefore, this is likely the reason for the small differences between the experimental and numerical force-deflection behaviors in Fig. 10, and also the slight differences in the moment–strain relationship in Fig. 10.

- The prestressing process for the UHPC beams and the camber deformation was captured in the numerical models using the surface traction method. Because the camber deflection was less than 0.2 in. (5 mm) and was measured in the field for the experimental studies, measurement errors may have affected the test results, which likely causes the difference between the experimental deflections and the numerical results. In addition, for beam 3, the camber deflection was measured before the HSC deck was placed on the UHPC beam. However, in the numerical simulation, the camber deflection was determined after the HSC deck was placed on the UHPC
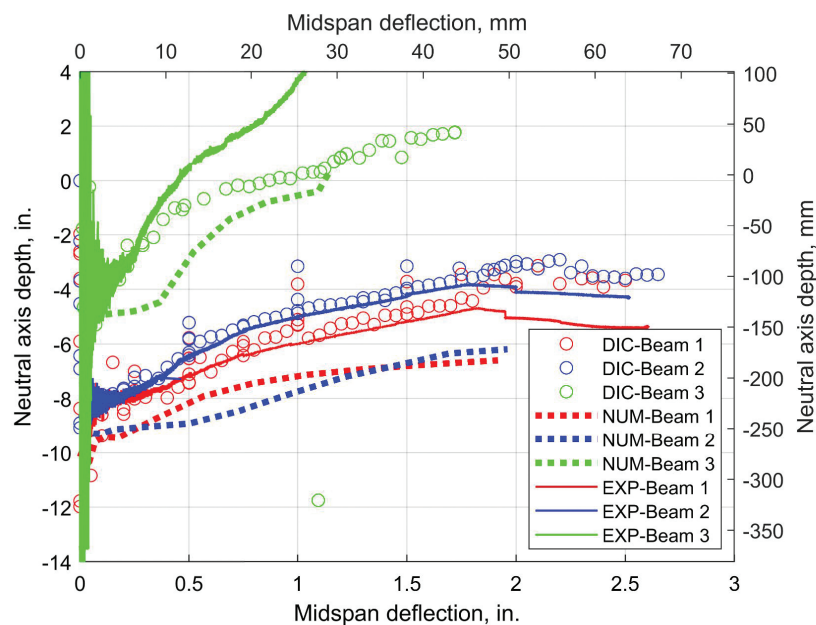


**Figure 11.** Location of neutral axis compared with midspan deflection for beam 1, beam 2, and beam 3. Note: DIC = digital image correlation; EXP = experimental data; NUM = numerical simulation.

beam, which caused the difference between the experimental and numerical analysis results. To further validate the prestressing process in the numerical model, the local behavior of the moment–strain curve and the location of neutral axis were compared. The good agreement between the experimental and numerical analysis results in Fig. 11 shows that the prestress is effectively and accurately transferred to the concrete in the numerical models. Thus, it was concluded that the simulation of the prestressing process is effective.

Surface traction was used as a new approach for applying prestressing force in the numerical simulation. This approach allows large prestressing forces to be applied without convergence problems.

The DIC results were compared with the numerical results, and the development of the strain on the UHPC beams was identical. The first cracking strain of concrete in the numerical model was close to the DIC results as well.

The practical implementation of prestressed UHPC beams can be predicted using the proposed numerical FE analysis method, which has been verified by comparing experimental results with numerical simulation in both global and local behaviors. The results indicate that the assumed analytical prediction model for the inelastic behavior of the UHPC is valid and can be used in numerical FE analysis. Similar models can be used to predict other related mechanical behaviors of concrete members for further research, such as flexural behavior of prestressed composite members and mechanical behavior of joints and overlays using UHPC.

## Acknowledgments

## References

1. Graybeal, B. A. 2015. "Compression Testing of Ultra-High-Performance Concrete." *Advances in Civil Engineering Materials* 4 (2): 102–112. https://doi.org/10.1520/ACEM20140027.

2. Graybeal, B. A. 2006. *Material Property Characterization of Ultra-High Performance Concrete*. Washington, DC: Federal Highway Administration.

3. AFGC-SETRA (Association Française de Génie Civil–Service d'étude des Transports, des Routes et de Leurs Aménagement). 2002. *Ultra High Performance Fibre-Reinforced Concretes, Interim Recommendations*. Bagneux, France: SETRA.

4. DAfStB (German Association for Reinforced Concrete) UHPC. 2005. *State-of-the-Art Report on Ultra High Performance Concrete—Concrete Technology and Design*. Berlin, Germany: DAfStB.

5. Orange, G., P. Acker, and C. Vernet. 1999. "A New Generation of UHP Concrete: Ductal Damage Resistance and Micromechanical Analysis." In *Proceedings of the 3rd International Rilem Workshop on High Performance Fibre Reinforced Cement Composites, Mainz*, edited by H. W. Reinhardt and A. E. Naaman, 101–111. Paris, France: RILEM.

6. Shafieifar, M., M. Farzad, and A. Azizinamini. 2018. "A Comparison of Existing Analytical Methods to Predict the Flexural Capacity of Ultra High Performance Concrete (UHPC) Beams." *Construction and Building Materials* 172 (30): 10–18. https://doi.org/10.1016/j.conbuildmat.2018.03.229.

7. Shafieifar, M., M. Farzad, and A. Azizinamini. 2017. "Experimental and Numerical Study on Mechanical Properties of Ultra High Performance Concrete (UHPC)." *Construction and Building Materials* 156 (15): 402–411. https://doi.org/10.1016/j.conbuildmat.2017.08.170.

8. Nasrin, S., and A. Ibrahim. 2018. "Finite-Element Modeling of UHPC Hybrid Bridge Deck Connections." *International Journal of Advanced Structural Engineering*, no. 10: 199–210. https://doi.org/10.1007/s40091-018-0192-2.

9. Singh, M., A. H. Sheikh, M. S. Mohamed Ali, P. Visintin, and M. C. Griffith. 2017. "Experimental and Numerical Study of the Flexural Behaviour of Ultra-High Performance Fibre Reinforced Concrete Beams." *Construction and Building Materials* 138 (1): 12–25. https://doi.org/10.1016/j.conbuildmat.2017.02.002.

10. Wang, C. Q., Y. F, Zhu, and Y. G. Shen. 2013. "Finite Element Analysis of Prestressed Steel Reinforced Concrete Beam." *Applied Mechanics and Materials*, no. 433–435: 2302–2308. https://doi.org/10.4028/www.scientific.net/AMM.433-435.2302.

11. Ren, W., L. H. Sneed, Y. Yang, and R. He. 2015. "Numerical Simulation of Prestressed Precast Concrete Bridge Deck Panels Using Damage Plasticity Model." *International Journal of Concrete Structures and Materials*, no. 9: 45–54. https://doi.org/10.1007/s40069-014-0091-2.

12. Newberry, C. M., J. M. Hoemann, B. T. Bewick, and J. S. Davidson. 2010. "Simulation of Prestressed Concrete Sandwich Panels Subjected to Blast Loads." In *Structures Congress 2010*. https://doi.org/10.1061/41130(369)163.

13. Chen, L., and B. A. Graybeal. 2011. "Modeling Structural

Performance of Ultrahigh Performance Concrete I-Girders." *Journal of Bridge Engineering* 17 (5): 754–764. https://doi.org/10.1061/(ASCE)BE.1943 -5592.0000305.

14. Van Meirvenne, K., W. De Corte, V. Boel, and L. Taerwe. "Overview and New Insights into the Modeling of the Force Transfer in the End Zones of Pretensioned Concrete Girders." In *Proceedings of the 12th fib International PhD Symposium in Civil Engineering, August 29–31, 2018, Prague, Czech Republic*. Lausanne, Switzerland: *fib* (International Federation for Structural Concrete).

15. Barzin Mobasher, A. L., Y. Yao, A. Arora, and N. Neithalath. 2021. "Characterization of Toughening Mechanisms in UHPC through Image Correlation and Inverse Analysis of Flexural Results." *Cement and Concrete Composites*, no. 2021: 122.

16. McGinnis, M. J., M. Holloman, M. Lisk, A. O'Donnell, and Y. C. Kurama. 2012. "3-D Digital Image Correlation—An Underused Asset for Structural Testing." In *Structures Congress* 2012. https://doi.org/10 .1061/9780784412367.172.

17. Giesler, A. J., M. J. McGinnis, and B. D. Weldon. 2018. "Flexural Behavior and Analysis of Prestressed Ultra-High-Performance Concrete Beams Made from Locally Available Materials." *PCI Journal* 63 (6): 66–80. https:// doi.org/10.15554/pcij63.6-02.

18. Giesler, A. J., S. Burl Applegate, and B. D. Weldon. 2016. "Implementing Nonproprietary, Ultra-High-Performance Concrete in a Precasting Plant." *PCI Journal* 61 (6): 68–80. https://doi.org/10.15554/pcij61.6-03.

19. Oller, S., E. Oñate, J. Oliver, and J. Lubliner. 1990. "Finite Element Nonlinear Analysis of Concrete Structures Using a 'Plastic-Damage Model.'" *Engineering Fracture Mechanics* 35 (1–3): 219–231. https://doi.org/10.1016/0013-7944(90)90200-Z.

20. Lubliner, J., J. Oliver, S. Oller, and E. Oñate. 1989. "A Plastic-Damage Model for Concrete." *International Journal of Solids and Structures* 25 (3): 299–326. https:// doi.org/10.1016/0020-7683(89)90050-4.

21. Lee, J., and G. L. Fenves. 1998. "Plastic-Damage Model for Cyclic Loading of Concrete Structures." *Journal of Engineering Mechanics* 124 (8): 892–900. https://doi .org/10.1061/(ASCE)0733-9399(1998)124:8(892).

22. Kupfer, H., H. K. Hilsdorf, and H. Rusch. 1969. "Behavior of Concrete Under Biaxial Stresses." *Journal of the American Concrete Institute* 66 (8): 656–666. https://doi.org/10.14359/7388.

23. Jankowiak, T., and T. Łodygowski. 2005. "Identification of Parameters of Concrete Damage Plasticity Constitutive Model." *Foundations of Civil and Environmental Engineering*, no. 6: 53–69.

24. Sümer, Y., and M. Aktaş. 2015. "Defining Parameters for Concrete Damage Plasticity Model." *Challenge Journal of Structural Mechanics* 1 (3): 149–155. https://doi.org /10.20528/cjsmec.2015.07.023.

25. Ray, T., and A. M. Reinhorn. 2014. "Enhanced Smooth Hysteretic Model with Degrading Properties." *Journal of Structural Engineering* 140 (1). https://doi.org/10.1061 /(ASCE)ST.1943-541X.0000798.

26. Weldon, B. D., D. V. Jáuregui, C. M. Newtson, C. W. Taylor, K. F. Montoya, S. Allena, J. Muro, M. Talahat, E. Lyell, and E. T. Visage. 2012. *Feasibility Analysis of Ultra High Performance Concrete for Prestressed Concrete Bridge Applications—Phase II*. Washington, DC: Transportation Research Board.

27. Lyell, E. K., J. Muro, C. M. Newtson, B. D. Weldon, D. V. Jauregui, and S. Allena. 2012. "Optimization of Ultra High Performance Concrete Mixture Proportions Using Locally Available Materials." In Proc., *12th Int. Conf. on Recent Advances in Concrete Technology and Sustainability Issues*. Red Hook, NY: Curran Associates Inc.

28. Visage, E. T., B. D. Weldon, D. V. Jauregui, and C. M. Newtson. 2019. "Flexural Performance of Ultrahigh-Performance Concrete Developed Using Local Materials." *Journal of Materials in Civil Engineering* 31 (5): 04019050. https://doi.org/10.1061/(ASCE)MT.1943 -5533.0002683.

29. Manglekar, H. C., E. T. Visage, and T. Ray. 2017. "Experimental and Analytical Investigations of a Locally Developed Ultrahigh-Performance Fiber-Reinforced Concrete." *Journal of Materials in Civil Engineering* 29 (2). https://doi.org/10.1061/(ASCE)MT.1943-5533 .0001732.

30. Giesler, A. J. 2014. "Flexural Behavior and Analysis of Prestressed Ultra-High-Performance Concrete Beams Made from Locally Available Materials." MS thesis, Department of Engineering, New Mexico State University. https://doi.org/10.15554/pcij63.6-02.

31. Manning, M. P., B. D. Weldon, M. J. McGinnis, D. V. Jáuregui, and C. M. Newtson. 2016. "Behavior Comparison of Prestressed Channel Girders from High-Performance and Ultrahigh-Performance Concrete." *Transportation Research Record: Journal of the Transportation Research Board* 2577, no.1. https://doi .org/10.3141/2577-08.

32. Guaderrama, L. R., and B. D. Weldon. 2013. *Compressive Stress-Strain Behavior of Ultra High Performance Concrete Using Local Materials*. Washington, DC: Transportation Research Board.

33. AASHTO (American Association of State and Highway Transportation Officials). 2012. *AASHTO LRFD Bridge Design Specifications*. 6th ed. Washington, DC: AASHTO.

## Notation

$A_{surface}$ = surface area of prestressing strands

$d_c$ = compressive damage variable

$d_t$ = tensile damage variable

$e$ = eccentricity of the plastic potential surface

$E_0$ = initial (undamaged) elastic stiffness of the material

$E_c$ = modulus of elasticity of concrete

$f$ = yield function

$\phantom{f}$ = concrete compressive strength

$f_{f,u}$ = tensile strength of the crack bridging fibers

$f_{pu}$ = ultimate tensile strength of prestressing strand

$f_{py}$ = yield strength of prestressing strand

$f_r$ = concrete modulus of rupture

$G$ = flow potential

$I$ = first invariant of stress

$K_c$ = ratio of compressive concrete strength under equal biaxial compression to triaxial compression

$\overline{p}$ = effective hydrostatic stress

$P$ = applied vertical load in four-point loading test

$P_{st}$ = prestressing force on prestressing strands

$\overline{q}$ = Mises equivalent effective stress

$\overline{S}$ = deviatoric part of the effective stress tensor $\overline{s}$

$S_1$ = the yield surface 1 on the deviatoric plane

$S_2$ = the yield surface 2 on the deviatoric plane

$S_3$ = the yield surface 3 on the deviatoric plane

$w/cm$ = water–cementitious material ratio

$\alpha$ = dimensionless constant

$\beta$ = dimensionless constant

$\gamma$ = dimensionless constant

$\varepsilon$ = strain

$\tilde{\varepsilon}^{pl}$ = equivalent plastic strain

$\varepsilon_c$ = compressive strain

$\varepsilon_c^{el}$ = compressive elastic strain

$\tilde{\varepsilon}_c^{pl}$ = compressive plastic strain

$\varepsilon_{f,lim}$ = limiting strain for fiber postcracking strength

$\varepsilon_t$ = tensile strain

$\varepsilon_t^{el}$ = tensile elastic strain

$\tilde{\varepsilon}_t^{pl}$ = tensile plastic strain

$f_c'$ = viscosity parameter

$\sigma$ = stress

$\sigma_{b0}$ = initial biaxial compressive yield stress

$\sigma_c$ = compressive stress

$\sigma_{c0}$ = initial uniaxial compressive yield stress

$\sigma_{cu}$ = the ultimate stress

$\sigma_t$ = tensile stress

$\sigma_{t0}$ = initial uniaxial tensile failure stress

$\overline{\sigma}$ = effective stress tensor

$\overline{\sigma}_c$ = effective compressive stress

$\overline{\sigma}_c\left(\tilde{\varepsilon}_c^{pl}\right)$ = effective compressive cohesion stress

$\overline{\sigma}_{max}$ = maximum principle effective stress

$\overline{\sigma}_t\left(\tilde{\varepsilon}_t^{pl}\right)$ = effective tensile cohesion stress

$\overrightarrow{\sigma}_{st}$ = applied surface traction on prestressing strands

$\hat{\overline{\sigma}}_1$ = uniaxial tension in one plane

$\hat{\overline{\sigma}}_2$ = uniaxial tension in another plane

$\hat{\sigma}_1$　　　= effective uniaxial tension in one plane
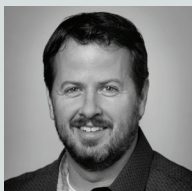
$\hat{\sigma}_2$　　　= effective uniaxial tension in another plane

$\psi$　　　= dilation angle

## About the authors

Wei Sun is a PhD candidate in the department of Civil Engineering at New Mexico State University in Las Cruces, N.Mex.

Brad D. Weldon is Henry Massman Teaching Professor of Civil Engineering in the department of Civil and Environmental Engineering and Earth Sciences at the University of Notre Dame in Notre Dame, Ind.

Michael J. McGinnis is dean of the School of Engineering and Engineering Technology at Letourneau University in Longview, Tex.

Ruinian Jiang is a professor in the department of Civil Engineering at New Mexico State University in Las Cruces, N.Mex.

## Abstract

This paper presents finite element simulations of the flexural behavior of three prestressed ultra-high-performance concrete (UHPC) beams based on the concrete damaged plasticity model (CDPM) available within Abaqus. A novel numerical model that applies the prestressing force through surface traction is proposed. The flexural deformation of the prestressed UHPC beams is simulated from the application of the prestressing force through failure under flexural loading. Material properties were measured and informed values for CDPM input parameters. The model was compared with four-point loading tests previously conducted to study the flexural behavior of large-scale prestressed UHPC beams. Digital image correlation (DIC), supplemented with traditional sensors, was used during the test to monitor behavior. The primary results based on the numerical modeling are as follows:

- The model is validated to accurately simulate the flexural behavior of prestressed UHPC beams, both in global deflection and local strain.

- The prestressing process, including camber deformations, is effectively simulated.

- The new approach to apply prestressing force in the model can be applied in scenarios requiring large prestressing forces.

- The numerical results are also validated through comparison with DIC results.

The new numerical modeling approach will be effective for guiding experimental studies and design of prestressed UHPC beam elements.

## Keywords

## Review policy

This paper was reviewed in accordance with the Precast/Prestressed Concrete Institute's peer-review process. The Precast/Prestressed Concrete Institute is not responsible for statements made by authors of papers in *PCI Journal*. No payment is offered.

## Publishing details

## Reader comments

Please address any reader comments to *PCI Journal* editor-in-chief Tom Klemens at tklemens@pci.org or Precast/Prestressed Concrete Institute, c/o *PCI Journal*, 8770 W. Bryn Mawr Ave., Suite 1150, Chicago, IL 60631. ⨆